Mechanistic investigations into the encapsulation and release of small molecules and proteins from a supramolecular nucleoside gel *in vitro* and *in vivo*

Maria Galini Faidra Angelerou[a], Robert Markus[b], Vasiliki Paraskevopoulou[a], Rugerro Foralosso[a], Philip Clarke[c], Clara V Alvarez[d], Miguel Chenlo[d], Litty Johnson[a], Catrin Rutland[e], Stephanie Allen[a], Christopher Brasnett[f], Annela Seddon[f,g], Mischa Zelzer[a,*], Maria Marlow[a,*]

[a] School of Pharmacy, University of Nottingham, UK
[b] SLIM Imaging Unit, Faculty of Medicine and Health Sciences, School of Life Sciences, University of Nottingham, Nottingham NG7 2RD, UK
[c] School of Medicine, University of Nottingham, Queen's Medical Centre, UK
[d] School of Medicine, University of Santiago de Compostela, Spain
[e] School of Veterinary Medicine and Science, Faculty of Medicine, University of Nottingham, Sutton Bonington, UK
[f] HH Wills Physics Laboratory, Tyndall Avenue, University of Bristol, BS8 1TL, UK
[g] Bristol Centre for Functional Nanomaterials, HH Wills Physics Laboratory, Tyndall Avenue, University of Bristol, BS8 1TL, UK

ARTICLE INFO

ABSTRACT

Supramolecular gels have recently emerged as promising biomaterials for the delivery of a wide range of bioactive molecules, from small hydrophobic drugs to large biomolecules such as proteins. Although it has been demonstrated that each encapsulated molecule has a different release profile from the hydrogel, so far diffusion and steric impediment have been identified as the only mechanisms for the release of molecules from supramolecular gels. Erosion of a supramolecular gel has not yet been reported to contribute to the release profiles of encapsulated molecules. Here, we use a novel nucleoside-based supramolecular gel as a drug delivery system for proteins with different properties and a hydrophobic dye and describe for the first time how these materials interact, encapsulate and eventually release bioactive molecules through an erosion-based process. Through fluorescence microscopy and spectroscopy as well as small angle X-ray scattering, we show that the encapsulated molecules directly interact with the hydrogel fibres - rather than being physically entrapped in the gel network. The ability of these materials to protect proteins against enzymatic degradation is also demonstrated here for the first time. In addition, the released proteins were proven to be functional *in vitro*. Real-time fluorescence microscopy together with macroscopic release studies confirm that erosion is the key release mechanism. *In vivo*, the gel completely degrades after two weeks and no signs of inflammation are detected, demonstrating its *in vivo* safety. By establishing the contribution of erosion as a key driving force behind the release of bioactive molecules from supramolecular gels, this work provides mechanistic insight into the way molecules with different properties are encapsulated and released from a nucleoside-based supramolecular gel and sets the basis for the design of more tailored supramolecular gels for drug delivery applications.

1. Introduction

Hydrogels for biomedical applications such as tissue engineering and drug delivery are widely reported [1–3]. Hydrogels are traditionally divided into polymeric gels that consist of covalently cross-linked polymer networks and supramolecular gels, consisting of fibrillar networks formed through non-covalent interactions [4]. Recently, supramolecular gels have attracted significant attention in drug delivery, especially in the delivery of biologics [5], where they have demonstrated numerous advantages over polymer based gels including the fine tuning of their properties through different stimuli; self-healing; and, mostly involve mild conditions of gelation that do not compromise the stability of sensitive biopharmaceutical molecules such as proteins and nucleic acids during encapsulation [6–8]. On the other hand, the crosslinking of polymeric gels can involve harsh conditions of gelation such as UV light or low pH to initiate cross-linking or the use of solvents

which has been proven detrimental for the functionality of bio-pharmaceuticals [9].

Bioinspired gelators based on peptides [10] and nucleic acids are popular candidates for drug delivery systems [7,11] because of their inherent biocompatibility due to their high water content and their self-healing properties [7]. For example Puramatrix®, a self-assembling acetyl-(Arg-Ala-Asp-Ala)$_4$-CONH$_2$ peptide that forms a stable hydrogel after increasing the pH and the ionic strength, has been employed for a broad range of clinical applications and has successfully delivered several biologically-active agents such as proteins (growth factors, cytokines, insulin or antibodies) and siRNA in preclinical *in vivo* studies [12–14]. Peptide-based gels, however, have been shown to be susceptible to proteolytic enzymatic degradation and chemical modifications are necessary to improve their biostability [15–17]. Nucleoside-based gelators are proposed as a novel alternative modality that would be stable against proteolytic enzymes.

Nucleoside-based gels have recently been introduced as injectable delivery systems that can reform *in situ* after injection at the site of action [18], delivering different classes of molecules from small therapeutic molecules to macromolecules such as proteins and nucleic acids [19,20]. For example, a guanosine-5′-hydrazide gel was able to encapsulate various pharmacologically active molecules such as acyclovir, vitamin C and vancomycin [21], whereas a 5′-deoxy-5′-iodoguanosine gel was reported to incorporate antivirals [22]. Additionally, Kaplan et al. demonstrated that a thymidine-based mechanoresponsive hydrogel can be used for the delivery of antibodies [19]. A urea based-bolamphiphile was found to avoid the foreign body reaction after *in vivo* injection, demonstrating the ability of these types of gels to be immunocompatible [18]. Ramin et al. reported the sustained release of a small hydrophobic fluorescent dye and a fluorescently labelled protein through a nucleotide lipid containing thymidine and 1,2 –dipalmitoyl-sn-glycerol phosphate paired with different cations with no toxicity *in vivo* [20]. Additionally this hydrogel was shown to protect the integrity of the model protein *in vivo* for a period of a few days compared to the non-formulated protein, successfully demonstrating the potential of these materials. Interestingly, the authors reported that, despite their size, the small hydrophobic molecule was released more slowly compared to the larger, more hydrophilic protein, raising questions over the influence that the properties of the molecules of interest can have on the encapsulation mechanism and the release behaviour of the final formulation.

Proteins are complex macromolecules with a diversity of chemical groups exposed on the surface or buried in their core depending on the nature of the surrounding environment. Two major properties that define their behavior in solution are their molecular weight (MW) and charge. Until now, protein release from supramolecular gels has been demonstrated to be strongly influenced by the proteins' MW and charge [23–25]. Mechanisms that have been identified to control the release of proteins from supramolecular gels including diffusion, electrostatic interactions and steric impediment through the hydrophilic pores created by the 3D nanofiber scaffold of the hydrogel [23–25]. In addition, our work [26] and that of others [27–29] has demonstrated that proteins encapsulated in supramolecular gels can be immobilised by the naonofiber scaffold through interactions with the hydrophobic core of the gel nanofibers. Hence, we postulate that this interaction of the protein with the gel nanofiber could have a significant effect on the protein release profile and, if this is the case, that the mechanism of protein release will be dominated by an erosion process. To date erosion based mechanisms have only been demonstrated for polymer hydrogels but not for supramolecular gels [9,30,31].

Herein, we use the well characterised, self-healing nucleoside-based hydrogelator *N*4-octanoyl-2′-deoxycytidine [32,33] developed in our group (SI, Fig. S1), to encapsulate a broad range of molecules (a small hydrophobic molecule and several proteins) and characterize its performance as a drug delivery system *in vivo* and *in vitro*. This nucleoside-based gelator was previously shown to encapsulate a hydrophobic dye

(model molecule for hydrophobic drugs) selectively into the hydrophobic core of the fibers [33]. Although others in the field have used nucleoside gelators for protein delivery [19,20], the novelty of this work is that we mechanistically investigate how proteins with different properties associate with the gel nanofibers and, for the first time for a supramolecular gel, we report the detailed mechanism of encapsulation and release of therapeutically relevant molecules and erosion of the gel. After release, we demonstrate that functional proteins (lysozyme and insulin) retain their biological activity *in vitro*. Furthermore, the ability of the gel to improve the stability of a model protein in the presence of proteolytic enzymes compared to the protein alone is demonstrated for the first time. Finally, the release of a small hydrophobic dye and a fluorescently labeled protein as well as their effect on the gel degradation profile are studied *in vitro* and *in vivo*.

2. Results and discussion

2.1. Encapsulation of proteins in hydrogels

In order to investigate the potential of the hydrogel to act as a drug delivery system for the controlled release of different proteins we incorporated four model proteins into the gel (SI, Fig. S2). Bovine Serum Albumin (BSA), β-lactoglobulin (β-lact) and insulin (ins) are negatively charged at physiological pH (PBS, pH 7.4) but possess different MWs whereas β-lactoglobulin and lysozyme (lys) have similar/comparable MWs but are negatively and positively charged, respectively, at physiological pH. Stable gels were obtained after encapsulation of all proteins, (SI, Fig. S3).

This hydrogelator has been previously reported to be self-healing [32]. This is an important condition for the syringeability of the gel and its ability to reform *in situ*. Rheology measurements have been extensively used in the literature to simulate the shear stress during syringing [18,24,32]. Here, we perform time dependent rheology measurements (SI, Fig. S4) which confirm that the presence of the protein is not preventing the ability of the gel to self-heal.

After establishing that a self-healing supramolecular gel can be formed with the *N*4-octanoyl-2′-deoxycytidine gelator in the presence of proteins with different MWs and charge we investigated how the proteins were entrapped within the gel. Previous literature has demonstrated that peptide based supramolecular hydrogels can immobilise proteins through the interaction of the protein with the hydrophobic core of the nanofiber [27–29] but physical entrapment of the proteins in the hydrophilic cavities of the nanofibrous gel network may also be possible in our system.

2.1.1. Protein-gel fibre association

In order to investigate the location of the proteins in the gel and elucidate the interaction between nanofibers and proteins we used fluorescence microscopy to image fluorescamine labelled proteins. Fluorescamine is a well-established dye in protein quantification as it reacts with primary amines and forms fluorescent complexes, consequently it is selective for the proteins and not the gelator [34]. In the presence of the labelled proteins, fibrous structures can be observed (Fig. 1) that are similar in appearance to the fibrous structure of the gel that was reported before [32]. As the gel fibers alone are not fluorescent (at λ_{ex} = 405 nm), the observation of fibres can be assumed to be caused by the association of fluorescent proteins with the gel fibre network. The dispersed points giving strong fluorescence signals across the fibre network are likely due to protein and/or dye associated with fibre bundles (crossover points) or dye/protein aggregates. Note that the size of the observed features does not correspond to their actual dimensions. The diameters of the fibers (254 nm) observed in fluorescence microscopy were considerably larger than expected (~13 nm) [33] which is attributed to instrumental limitations (Raleigh/Abbe criteria, signal to background and signal to noise (of the detector) ratio).
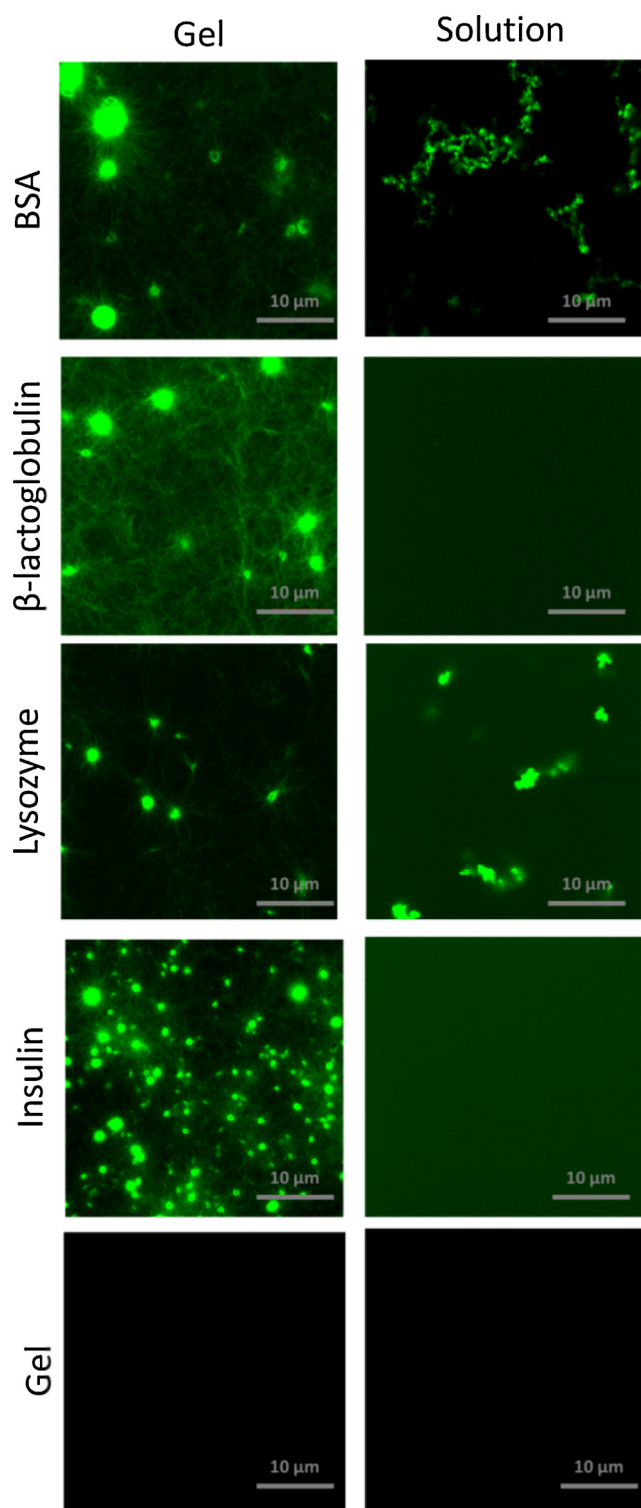
Fig. 1. Fluorescence images of gels (concentration 0.5% w/v) (left column) and solutions (right column) containing (30 μM) protein labelled with fluorescamine in PBS for 4 h at 37 °C; BSA, β-lactoglobulin, lysozyme, insulin and gel alone (from top to bottom). The 405 nm laser was set to 0.8%, emission detected at: 490–624 nm, channel colour (LUT) was set to green. (For interpretation of the references to colour in this figure legend, the reader is referred to the web version of this article).

2.1.2. Hydrophobic protein-gel fibre interactions

The intrinsic fluorescence of both the proteins and the gel was used for further evaluation of the interaction of the protein with the fibers

[35]. The protein's intrinsic fluorescence is due to the presence of aromatic amino acids and a change in their surrounding environment can result in a change in the fluorescence intensity or emission maxima [35]. The gelator is non-fluorescent in solution but it fluoresces in the self-assembled state, as previously reported [33]. As presented in Fig. 2, emission spectra were recorded for the gel after the encapsulation of the proteins, the gel and the proteins alone, after excitation at two wavelengths that have been widely used for the excitation of proteins, 275 nm for the general excitation of the three aromatic amino acids and 295 nm for the specific excitation of tryptophan (human insulin has no tryptophan, so no emission after excitation at 295 nm is detected).

Compared to the spectra obtained from protein solutions, the fluorescence emission spectra of all four different proteins in the gels shift and fully overlap with the emission spectra of the gel without the proteins. This suggests that the protein's intrinsic fluorescence is fully quenched due to their association with the fibers and only the fluorescence of the gel is detected. This may be the result of a change in the environment of the aromatic amino acids in the protein structure and indicates that these aromatic amino acids are directly involved in the fiber-protein interactions.

2.1.3. Small angle X-ray scattering studies

To understand if the presence of the protein is affecting the structure of the fibres, we performed small angle X-ray scattering (SAXS) measurements of the gels with proteins, the proteins in solution and the gel alone to determine the gel fiber diameters (Figs. 3 and SI S6). SAXS has been previously used to investigate the structures of supramolecular gels [33,36,37] as well as the effect that molecules encapsulated in the fiber have on the fiber diameter [38]. The gel sample was fitted to a flexible cylinder model (as previously reported for similar systems) [38], revealing a fiber radius of 73.2 Å, in good agreement with previously published data [33]. Since fluorescence microscopy images showed that the proteins locate themselves on the fibres yielding cylindrical geometries, the SAXS patterns obtained from protein containing gels were fitted to a flexible cylinder model in the same manner as the gel sample that did not contain proteins, yielding fibre radii of 91.2 ± 0.4 Å (BSA), 66.6 ± 0.4 Å (β-lactoglobulin), 71.1 ± 0.9 Å (lysozyme) and 67.6 ± 0.9 Å (insulin). The fitting parameters are presented in SI, Table S1. All fiber diameters cluster around the same range of values except that for the BSA containing gel. This indicates that there is an ordered association of BSA with the fiber. The other proteins likely associate with the fibers by arranging themselves in a non-ordered, amorphous structure surrounding the main gel fiber which would not be detectable by X-ray scattering. Together, the fluorescence microscopy and spectroscopy as well as the SAXS data (for BSA) provide complementary evidence that the proteins are not loosely entrapped in hydrophilic cavities between the gel fibres. Instead, the proteins engage in interactions with the gel fibers that result in a close association and co-localisation of the proteins and the fibers.

2.2. Prevention of protein enzymatic degradation

As one of the main drivers of protein encapsulation in gels is to protect them from enzymatic degradation, we subsequently evaluated whether the protein-gel association could be beneficial in preventing enzymatic degradation of the proteins. We have previously shown that the nucleoside gels used here are able to protect proteins from pH induced denaturation [26]. The ability of gels to provide protection against enzymatic degradation has been extensively suggested but never clearly demonstrated. Here, we exposed the BSA containing gels to two model proteolytic enzymes, α-chymotrypsin [39] and pepsin [40]. These enzymes are encountered in the human body, are readily available and inexpensive. Bovine Serum Albumin was chosen as the model protein due to its relative high molecular weight that would allow for a clear demonstration of the protein breakdown into shorter protein fragments in SDS-PAGE separation.
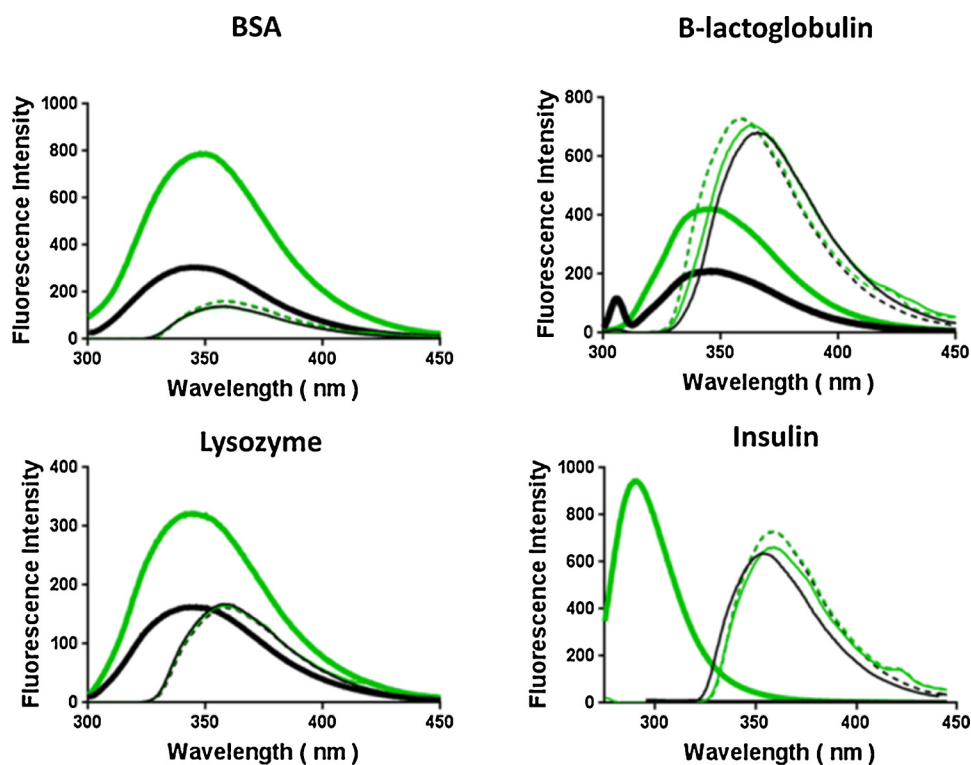
BSA

B-lactoglobulin

Lysozyme

Insulin

Fig. 2. Fluorescence emission spectra for gels (at concentration 0.5% w/v) containing four different proteins (30 μM) and the gel alone in PBS (30 μM for all proteins in gel and solution, apart from insulin which is 3 μM to allow recording of samples of insulin in gel and solution with the same instrumental settings). In every graph, protein containing gel after excitation at 295 nm (black solid), protein containing gel after excitation at 275 nm (green solid), protein in solution after at 295 nm (black bold), protein in solution after excitation at 275 nm (green bold), gel without protein after excitation at 295 nm (black dashed), gel without protein after excitation at 275 nm (green dashed). The two minor peaks between 400 nm and 450 nm on the spectra of the gels containing β-lacto-globulin and insulin have been identified as artefacts and are not related to the protein/gel intrinsic fluorescence. (For interpretation of the references to colour in this figure legend, the reader is referred to the web version of this article).
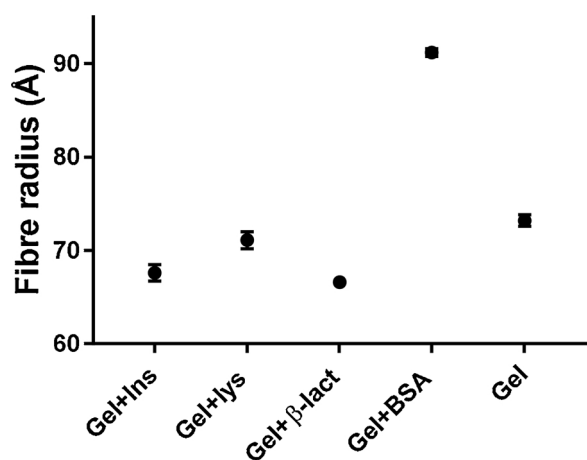

Fig. 3. Fibre radii determined from SAXS data obtained from gels (at concentration 0.5% w/v) with the four different proteins (30 μM) and the gel alone in PBS at room temperature. The data points represent the average fitted values of the radii and standard errors of the fitted values are also presented as error bars.

Samples of gels containing proteins (G) and samples of the protein in solution alone (P) were incubated for different time periods (1 h, 4 h and 1 day) in the presence of enzymes before analysing them using SDS-PAGE (Fig. 4). When the band that corresponds to BSA (highlighted in Fig. 4) was compared between samples containing protein only and protein in the presence of the gel, it is evident that for both enzymes the band intensity and hence the amount of intact protein for the protein alone was notably lower than for the protein/gel sample at all time points. At the later time points, the band intensity faded for the protein in the gel as well. This indicates that even though BSA degrades in both samples, the degradation process is considerably slower in the gel containing system, supporting the supposition that the presence of the gel has a protective effect on enzymatic degradation. The eventual decrease in the total amount of protein in the gel sample could be attributed to enzymes slowly diffusing into the gel, BSA partially diffusing out of the gel, the gel slowly eroding or a combination of all three processes.

2.3. Protein release and gel erosion

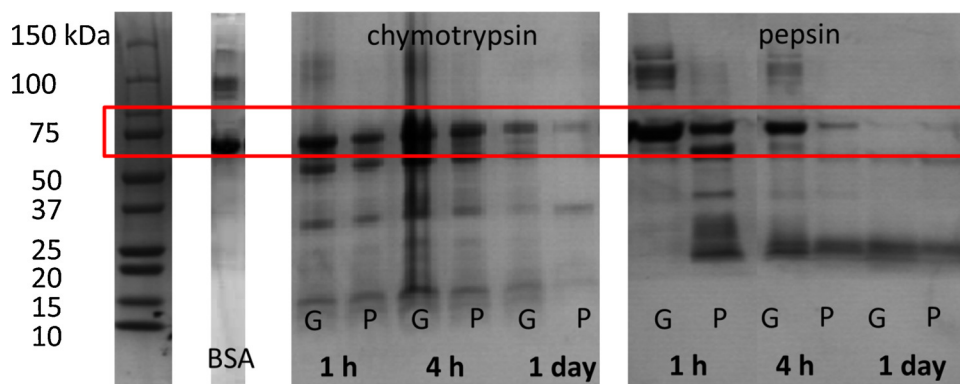The close association of the proteins with the gel fibres allows for

Fig. 4. SDS-PAGE for BSA (30 μM) encapsulated in gels (G) and BSA alone (P) after incubation with two different enzymes; chymotrypsin and pepsin for 1 h, 4 h and 1 day. In 120 μL of gel (0.5% w/v) in different buffers (50 mM KH_2PO_4 (pH = 4.5) for pepsin and PBS for chymotrypsin), 10 μL (5 mg/ml, ≥1250 units/mg) of pepsin and 20 μL (2 mg/ml, ≥80 units/mg) of chymotrypsin were pipetted on top of the already formed gel and incubated at 37 °C.
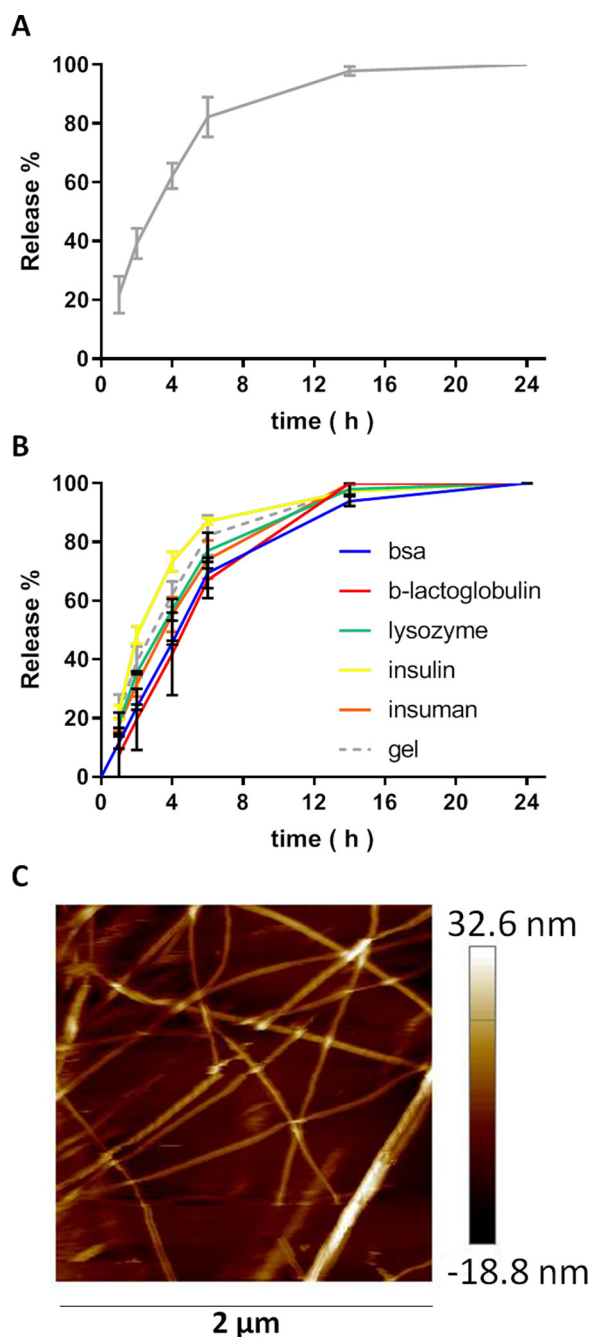
Fig. 5. Formation of stable, self-healing gels able to deliver different proteins in a sustained way. (A) Release profiles of gel alone (grey trace) and (B) Release profiles of different proteins from the gel; blue (BSA), β-lactoglobulin (red), lysozyme (green), insulin (yellow) and gel alone (dashed grey trace). 0.5 ml of protein containing (30 μM) gel (0.5% w/v) were incubated with 1 ml PBS at 37 °C. The protein concentration was determined at certain time points using a Bradford assay at 595 nm [41]. The gelator concentration was determined at 295 nm. (C) AFM images of gel fibers (gel alone at concentration 0.5% w/v) on mica imaged in the release medium (PBS) after 4 h incubation at 37 °C. 0.5 ml of gel (0.5% w/v) were incubated with 1 ml PBS at 37 °C. (For interpretation of the references to colour in this figure legend, the reader is referred to the web version of this article).

two possibile mechanisms (or a combination of both) of protein release from the system; dissociation of the protein from the fibers and diffusion out of the gel or degradation of the gel structure where the breakdown of the fiber structure ultimately results in the liberation of the proteins. We therefore investigated the *in vitro* release of the same

set of proteins (BSA, β-lact, ins and lys) from the gels. Gels without (Fig. 5A) and with the proteins (Fig. 5B) were brought in contact with PBS at 37 °C and samples of the supernatant were taken at different time points. The concentration of the proteins at each time point was determined using the colorimetric Bradford assay, measuring the absorbance at 595 nm [41] and the gelator concentration was quantified through its UV absorbance at 295 nm (Fig. 5A).

Interestingly, the release profiles of all proteins followed the same trend, regardless of the different protein properties (Fig. 5B). Notably, the release profile also matched the profile of the physical degradation of the gel, suggesting that gel degradation may be a key release mechanism for proteins from this system. For polymeric gels both diffusion and erosion/degradation have been reported to regulate the release depending on the formulation [9]. For example, for Pluronic gels encapsulating the therapeutic proteins insulin [30] and IL-2 [31], it was demonstrated that gel erosion underpins the release mechanism. To date, for supramolecular gels the protein release mechanisms have been identified as diffusion out of the gel, with contributions from electrostatic interactions and steric impediment [23–25] whereas gel erosion has not been reported so far. Especially for supramolecular peptide-based gels, it has been previously demonstrated that proteins with different properties mainly diffused through the gel and had different release profiles depending on their properties [24], whereas no data have been reported so far on the release mechanism of nucleoside-based gels. For this nucleoside-based gel, the correlation of the kinetics of the protein release and gel degradation profile as well as the independence of the release profile on the type of the encapsulated protein, strongly suggest that erosion is the main mechanism by which proteins leave the gel. Macroscopic images of the gel eroding over time are presented in SI, Fig. S7.

In order to study the gel erosion on the nanoscale, we used Atomic Force Microscopy (AFM). Gels not containing proteins were incubated in PBS at 37 °C and after 4 h incubation samples drawn from the supernatant were imaged with AFM at 37 °C in PBS. Individual fibers were captured floating in the supernatant (Fig. 5C) demonstrating that intact fibers leave the bulk gel during gel erosion in a biologically relevant environment. Complementary data using fluorescence imaging that shows gel erosion in the presence of labelled BSA will be discussed in a later section.

2.3.1. Investigating the released protein functionality

After evaluating that the gel provides sustained release a critical question is whether the functionality of the protein is preserved after encapsulation within the gel. This has also been a controversial topic for the polymeric gels [9]. Firstly, the integrity of all released proteins was tested with SDS-PAGE separation. As presented in Fig. 6A, all four released proteins have the same molecular weight as the proteins that did not undergo gel encapsulation (represented by the same band on the SDS-PAGE). Furthermore, the protein functionality is highly dependent on its secondary structure [42]. While circular dichroism would be a typical choice to study the secondary structure of proteins, in this system the strong CD activity of the gelator precludes the use of CD for the protein characterisation [33]. Considering this, we included a therapeutic protein, insulin and an enzyme, lysozyme in our study and assessed their activity after encapsulation [43].

2.3.1.1. Insulin functionality. To assess the bioactivity of insulin after the release through the gel, we used a cell-based functional assay. The HepG2 cells originate from a human liver carcinoma (one main target organ of insulin) and express abundant levels of the insulin receptor. A luciferase vector was transfected under the promoter fragment of the HMG CoA enzyme that is responsive to insulin [44–46]. The cell response to different doses of released insulin and insulin in solution was measured through luciferase activity. In Fig. 6B, insulin released from the gel (red bars) is plotted against insulin in solution (green bars). No difference between the bioactivity of the natural insulin and the
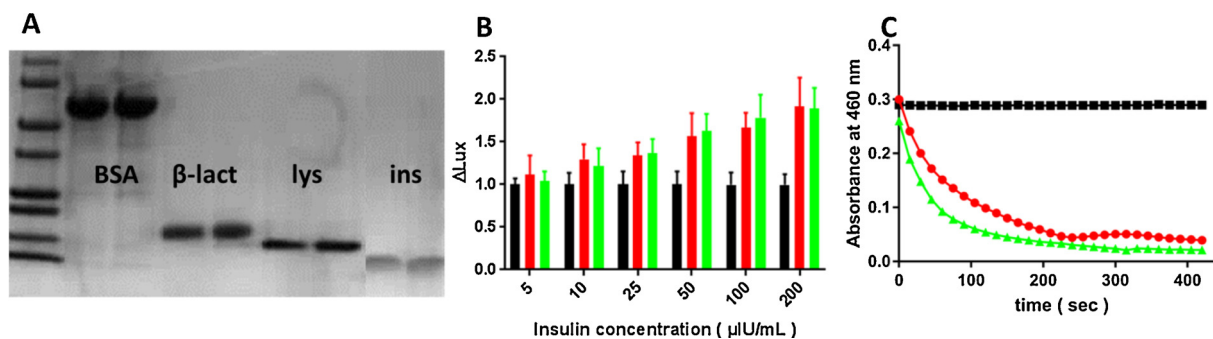
Fig. 6. SDS-PAGE of different proteins (30 μM) BSA, β-lactoglobulin (β-lact), lysozyme (lys), insulin (ins) after encapsulation in the gel (0.5% w/v). Data are presented in pairs (first column control protein and second released protein). Dose response curve for human insulin was measured through luciferase activity; [50] gel alone (black trace), insulin released from gel in the presence of gelator (red trace) and insulin alone (green trace) (N = 3 with 6 replicate measurements each). Turbidimetric assay of lysozyme; absorbance at 460 nm of *Micrococcus Lisodeikticus* lyophilised cell walls in the presence of gel alone (black trace), released protein (red trace) in the presence of gel, lysozyme control (green trace),(N = 3). (For interpretation of the references to colour in this figure legend, the reader is referred to the web version of this article).

released insulin was observed and, importantly a clear dose-response was observed at ranges of concentration similar to those present in humans, both at fasting (normal range 2–25 μUI/ml taken as a reference the Mayo Clinic laboratory fasting values for the normal population [47]) and at post-prandial levels (approximately 30–230 μIU/ml [48]). There was no action of the released insulin on the mutated promoter bearing four point-mutations, where also there was no action of the natural insulin, indicating that the response was specific for the insulin receptor (SI, Fig. S8).

2.3.1.2. Lysozyme functionality. Lysozyme is an antimicrobial enzyme that selectively cleaves β-1,4-glycosidic bonds between *N*-acetylmuramic acid and *N*-acetylglucosamine present in bacterial cell walls [49]. The functionality of lysozyme has been previously assessed using *Micrococcus lisodeikticus* lyophilised cell walls as a substrate [43]. The lytic activities of the released lysozyme after encapsulation in the gel and free lysozyme are presented in Fig. 6C. Both traces (green and red) follow the same trend and are both distinctly different from the control (black trace), demonstrating that released lysozyme has the similar activity as free lysozyme. Incubation of the cells with the gelator alone did not cause a change in absorbance, indicating that the gelator does not affect the integrity of the cell wall and that a change in absorbance in the gelator/protein sample is due to lysozyme released from the gel.

2.4. Release of small molecules and proteins

Upon demonstrating the ability of this hydrogel to sustain controlled release of functional proteins *in vitro*, we progressed to an assessment of the protein release *in vivo* using a fluorescently labelled protein (cyanine 5-BSA, Cy5-BSA). Our previous work has shown that a small hydrophobic dye can be encapsulated in the hydrophobic core of the fibers of this gelator [33]. Alongside the fluorescently labelled protein, we therefore also tested the release of a fluorescent dye (1,1′-dioctadecyl-3,3,3′,3′-tetramethylindocarbocyanine perchlorate, Dil) incorporated in the hydrophobic core of the nanofibers as a model for a small molecule hydrophobic drug molecule. The fluorescent probes were selected due to their good contrast in the *In Vivo* Imaging System (IVIS)® we employed. The purpose of these experiments is to investigate the release profiles of Cy5-BSA *in vivo* and the biocompatibility of the gel. Before moving to the *in vivo* experiments, we monitored the Cy5-BSA and Dil containing gels with fluorescence microscopy, investigating their release behaviour *in vitro* to help understand their *in vivo* behaviour.

2.4.1. Fluorescently labelled protein and fluorescent dye release in vitro

Real time fluorescence microscopy was used to follow the release of the encapsulated molecules from the gel *in vitro*. Gels containing either Dil or Cy5-BSA were prepared and incubated in PBS at 37°C for 48 h. Images were captured at t = 0 min, 10min, 24 h and 48 h and are presented Fig. 7. For t = 0 min, the fluorescent molecules directly associate with the fibers in both samples. It is important to highlight again that the gel alone was not fluorescent and the fluorescence signal can be exclusively associated with the presence of the encapsulated molecule (Cy5-BSA or Dil).

At t = 0 min, both samples show an extensive fluorescent network of fibers with dispersed points giving strong fluorescence signals, most likely due to protein and/or dye associated with fibre bundles (crossover points) or dye/protein aggregates (note that the size of the observed features does not correspond to their actual dimensions due to the method's limitations). After 10 min, we focused on the gel-PBS interface, where fluorescent fibers and protein aggregates were observed to be present on the outside of the bulk gel, suggesting that the protein aggregates were released from the gel (Fig. 7, zoom in at 10 min).

A similar observation was made with Dil encapsulated in the gel where fluorescent fibers as well as dye aggregates are found on the outside of the bulk gel. After 1 day, in both cases the bulk gel had been fully eroded leaving smaller gel fragments floating in the medium. In the case of Cy5-BSA, fluorescent structures of different sizes (< 20 μm) and shapes were floating in the medium whereas in the case of Dil encapsulating gel, significantly larger gel fragments were visible with diameters of more than 100 μm, suggesting that fibers are held together for longer in the latter. In the case of Dil encapsulating gel fragments, fibers were protruding out from the gel phase into the gel-medium interface, suggesting that interfacial erosion of the gel occurs through the loss of single fibers from the gel phase (SI, Fig. S9).

This data corroborates the *in vitro* protein release data above (Fig. 5B) that showed that the release of different encapsulated proteins from the gel followed the degradation of the gel.

In the case of the encapsulated hydrophobic dye (Dil), *in vitro* release data were impossible to acquire due to the high hydrophobicity of the dye that tended to interact strongly with the containers and not remain in solution. Even when different solvents were used to extract the dye, exact quantification was not possible. The use of an alternative dye was not an option at this stage as in contrast to other dyes Dil demonstrated selective binding into the hydrophobic cavity of the fibers and provided adequate contrast for the subsequent IVIS® study. Due to this, macroscopic images of the degradation of the gel encapsulating the dye and the gel alone are presented in Fig. S10, SI, over a course of 24 h. As the volume of the gel encapsulating Dil and the gel alone reduced in a similar manner over time, we assume that the release
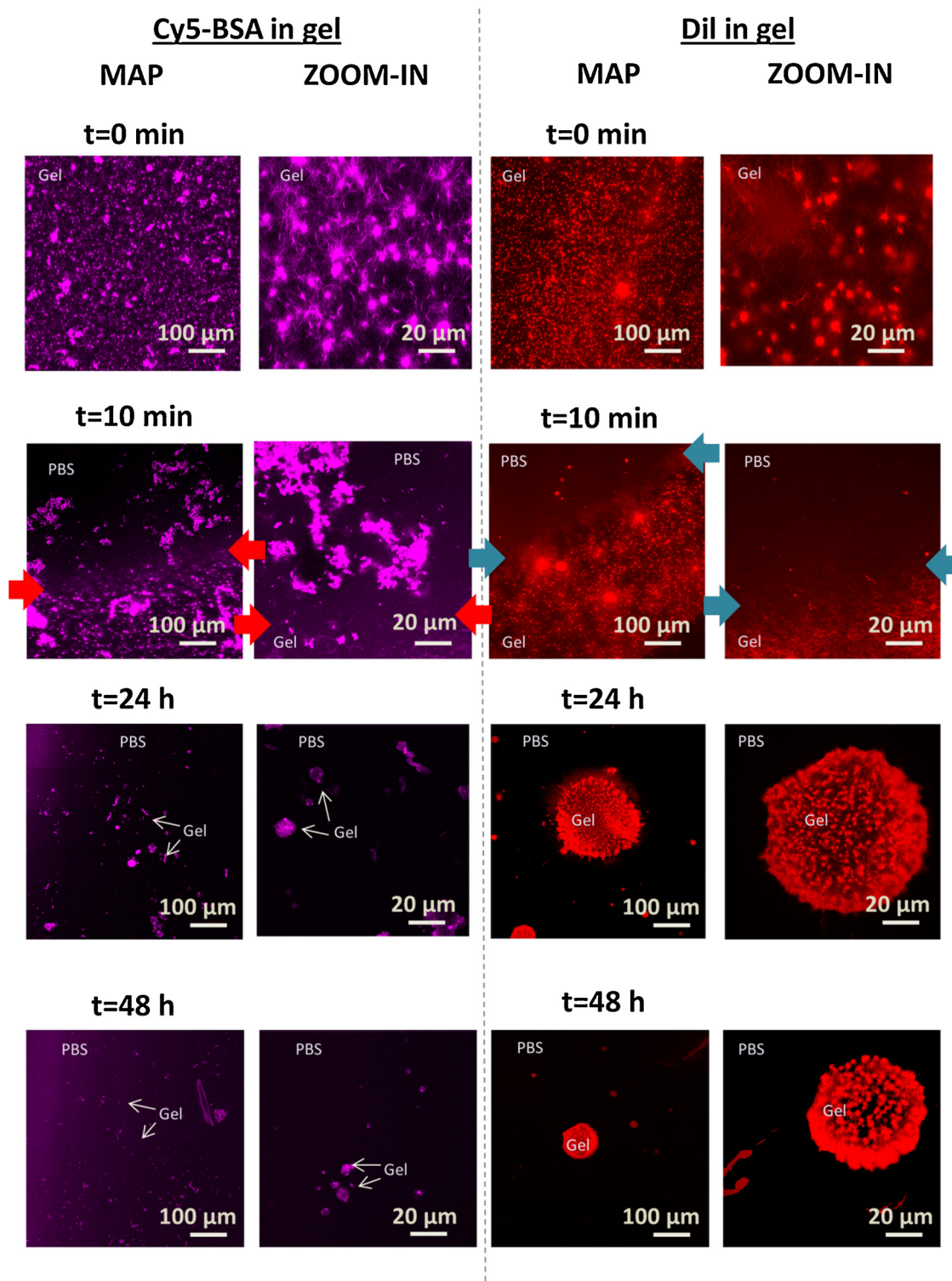
Fig. 7. Fluorescence microscopy images of gels (0.5% w/v) encapsulating Cy5-BSA at a final concentration of 15 μM (left) and hydrophobic dye (Dil) at a final concentration of 8.3 μM (right) at after incubation with PBS at 37 °C at different time points (t = 0 min, 10 min, 24 h, 48 h). The arrows indicate the gel-PBS interface. In each case a large area image (map) and a zoom in image were recorded. For the Cy5 labelled protein, 647 nm laser was set to 4%, emission detected at 654–752 nm, channel colour (LUT) was set to magenta; for Dil, 561 nm laser was set to 0.1%, emission detected at.561–624 nm.

of the dye follows the gel erosion as well and the gel completely degrades macroscopically within 1 day. The *in vitro* release data (Fig. 5B) are in good agreement with the fluorescence microscopy images that show gel breakdown within 24 h. The fluorescence microscopy images showed that the gel encapsulating the dye and the gel encapsulating the protein followed two different breakdown pathways; the first broke down into gel particles whereas the second into fibre bundles, suggesting that the forces holding the fibers together for the gel encapsulating the dye are stronger compared to the gel encapsulating the protein.
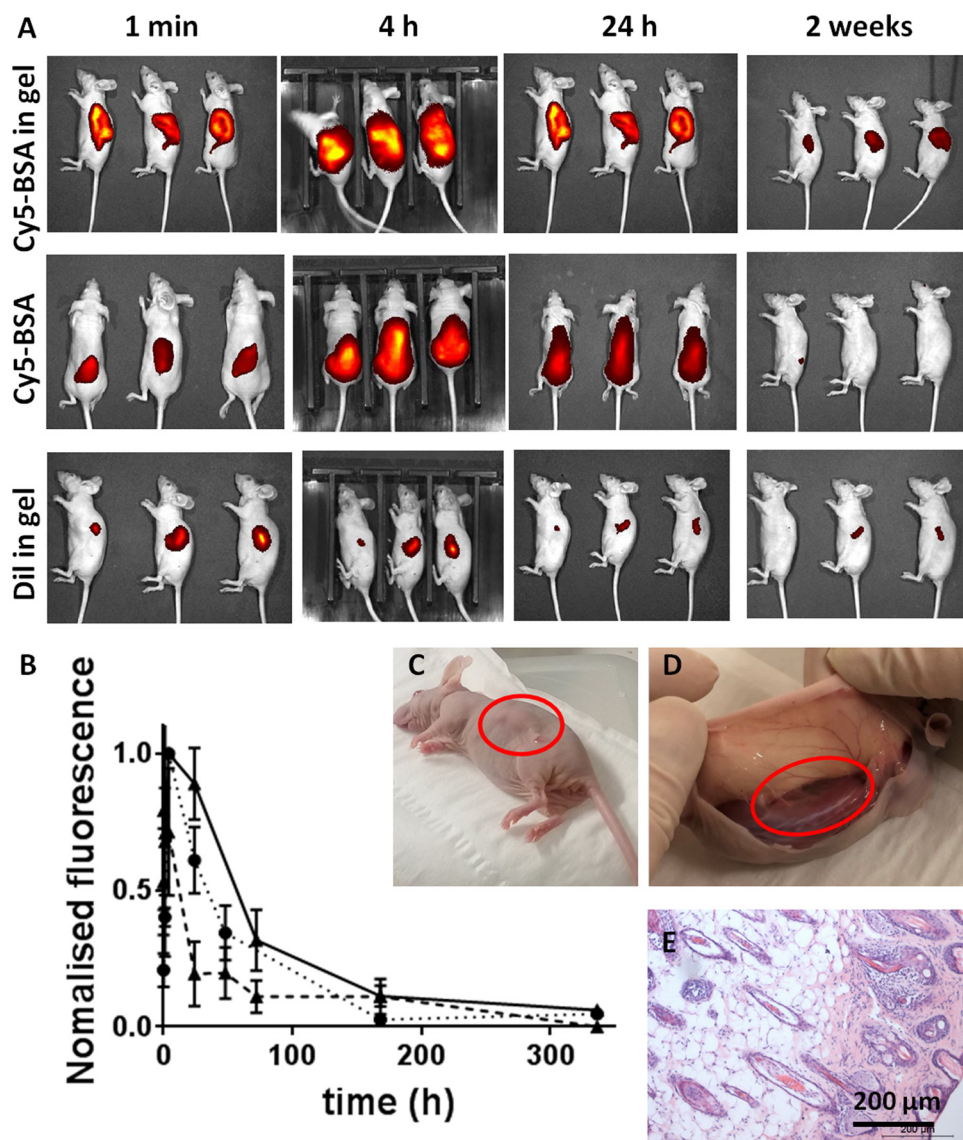
Fig. 8. *In vivo* data of gels encapsulating DiI and Cy5-BSA after subcutaneous injection in mice (N = 3 for each group); (A) IVIS® images of the mice after injection of 300 µl of gel (0.5% w/v) encapsulating Cy5-BSA (15 µM, top row), Cy5-BSA in solution (15 µM) and gel encapsulating a hydrophobic dye, DiI (8 µM). Images are presented in the same colour scale 6.00×10^8 - 1.00×10^{10} (ρ/sec/cm²/sr) for the gel encapsulating Cy5-BSA and Cy5-BSA in solution and 3.50×10^8 - 7.00×10^9 (ρ/sec/cm²/sr) for all the images of the gel with DiI. (B) Normalised to maximum fluorescence intensity (fluorescence signal is measured in radiance over the same region of interest for all images) of gel encapsulating Cy5-BSA (solid trace) and Cy5-BSA in solution (dotted trace) and gel encapsulating DiI (dashed trace) (N = 3). (C) Macroscopic image of tissue where control gel (without encapsulated molecule) was injected (D) Macroscopic image of tissue where control gel (without encapsulated molecule) was injected; after two weeks the animals were sacrificed and the gel had completely degraded. No control group was injected as DiI is highly hydrophobic and remains completely insoluble in PBS. The injection site is highlighted in red. (E) Photomicrograph showing normal cellular and tissue morphology. Haematoxylin and eosin were used to stain the tissue at and around the injection site 2 weeks after the injection of the control gel (without encapsulated molecule). Further photomicrographs and the control as given in the SI -Figs. S15 and S16 respectively. (For interpretation of the references to colour in this figure legend, the reader is referred to the web version of this article).

2.4.2. Fluorescently labelled protein and fluorescent dye release in vivo

To obtain a preliminary insight into the safety of the material *in vivo* and its potential as a drug delivery system, we performed IVIS® imaging following similar studies in the literature [20]. To date, a limited number of nucleoside-based gelators have been tested *in vivo* [18,20]. In this work, we used a nucleoside-based gel encapsulating a small hydrophobic dye (DiI) or Cy5-BSA in order to evaluate the release of these model molecules from the gel *in vivo*.

Hydrogels containing Cy5-BSA and DiI, Cy5-BSA in solution and gel alone were injected subcutaneously into mice. In Fig. 8A, IVIS® images of the mice are presented at different time points (0 h, 1 h, 24 h and 2 weeks after subcutaneous injection) for gels encapsulating Cy5-BSA (top) and DiI (bottom). In both cases the fluorescence intensity faded out over time and was almost zero after two weeks (very low levels of fluorescence were detected probably due to association of the dye with tissue). No control group was injected with DiI in solution as DiI is highly hydrophobic and remains completely insoluble in PBS. Fluorescence data of the encapsulated molecules were extracted for quantification and are presented in Fig. 8B. In all cases there was an increase in the fluorescence intensity of the encapsulated molecules during the first 4 h, probably due to the gel reformation after the shear stress applied during injection. Another explanation could be equilibration phenomena of the fluorescent probe in the lipophilic tissue

environment that have been previously reported [51]. After this period, fluorescence intensity started to drop as expected.

Fluorescence data of the gel containing Cy5-BSA and Cy5-BSA in solution (Fig. 8B) suggests that encapsulation in the gel increased retention of Cy5-BSA compared to Cy5-BSA in solution. In both cases, the mice of both groups were healthy when sacrificed after 2 weeks and there was no macroscopic trace of the gel in the tissue, indicating that the gel is biodegradable *in vivo* (Fig. 8D).

2.5. Biocompatibility in vivo

In order to investigate if the gel causes any inflammation, cross-sections of the tissue at the site of injection and surrounding the site of injection of the gel alone were stained with haematoxylin and eosin imaged as shown in Figs. 8D and S15. Tissue and cell morphology throughout the entire area of all samples appeared comparable to the control (Fig. S16). There was no evidence of the gel depot itself or of cellular or tissue damage from the gel in the samples. Areas of haemorrhage or excessive immune cell infiltration (including cells such as mononuclear leukocytes and polymorphonuclear cells) were not visualised within any of the tissues assessed. The basic histological investigations indicated no damage to the cells within the tissue where the gel had resided. These samples were measured 2 weeks after

injection, therefore, at this stage we can conclude that no chronic inflammation or tissue necrosis was observed, suggesting that the material does not cause any permanent damage to tissue. It is possible that an immune cell response could have been present in the days immediately following injection as is usual following injections of biomaterials [52–55].

3. Conclusions

Supramolecular gels have emerged as promising biomaterials for drug delivery. Here, we demonstrate that nucleoside-based supramolecular materials form stable, self-healing gels in the presence of incorporated proteins. We report for the first time that gel erosion plays a key part in the release mechanism of proteins from a supramolecular gel and provides indicative evidence that this erosion based release process is related to the non-covalent association of proteins to the gel fibres. Interestingly, the erosion-based release profile of the proteins is independent of the type of proteins used. Protection from enzymatic degradation was shown to be a major advantage of these materials for protein delivery. Additionally, after *in vitro* release, proteins (such as lysozyme and insulin) are shown to maintain their functionality. *In vivo* injection of the nucleoside based hydrogel resulted in no toxicity over two weeks and no signs of inflammation were detected. This highlights the suitability of supramolecular hydrogels to act as protective matrices for protein delivery and suggests that they could be used to release proteins in a manner that is independent of the nature of the proteins.

4. Experimental methods

4.1. Materials

2′-Deoxycytidine (lot #SLBN6031, 99% [high-performance liquid chromatography (HPLC)]), pepsin from porcine gastric mucosa (#P7012, lyophilized powder, ≥2,500 units/mg protein (E1%/280)), lysozyme from chicken egg white lyophilized powder (product # L6876, protein ≥90%, ≥40,000 units/mg protein), β-lactoglobulin B from bovine milk (≥90% (PAGE) product # L8005), Bovine Serum Albumin lyophilised powder, essentially fatty acid free and essentially globulin free, ≥99% ((agarose gel electrophoresis), product #A028) 1,1′-Dioctadecyl-3,3,3′,3′-tetramethylindocarbocyanine perchlorate 97% (product #468495) and fluorescamine [(product # 47614) BioReagent, suitable for fluorescence, ≥99.0% (UV)], C4129 α-Chymotrypsin from bovine pancreas, Type II, lyophilized powder, ≥40 units/mg protein, (product # C4129), Micrococcus lisodeikticus lyophilised cells, Dulbecco's Phosphate Buffered Saline Modified, (without calcium chloride and magnesium chloride, liquid, sterile-filtered, suitable for cell culture D8537) were purchased from Sigma Aldrich. Polyacrylamide gels 4–20% Mini-PROTEAN® TGX™ Precast Protein Gels, 12-well, 20 µl (#4561095) and Quick Start™ and Bradford 1x Dye Reagent (#5000205) were purchased from Bio-Rad. Cyanine5 NHS ester was purchased from Lumiprobe. Insuman Rapid 100 IU/ml solution for injection in a cartridge was purchased from Sanofi. SnakeSkin™ Dialysis Tubing was purchased from Thermofisher Scientific (Waltham, Massachusetts, United States), MWCO 3.5 kDa. For Fluorescence Microscopy Cellview cell culture slide (Item No.: 543079) were purchased from Greiner Bio-one. The gelator was synthesized according to previously published work. Analysis of the gelator was performed by NMR and liquid chromatography–mass spectrometry (LC–MS) (Supporting Information Figs. S12 and S13), and purity was determined as 98% (LC–MS). [32]

4.2. Gel preparation

Certain amount of gelator was weighed out in 2 ml HPLC vial and dispersed with PBS in order to get a final concentration of 0.5% w/v. The vial was carefully sealed and the gelator was heated up to 100 °C

till complete dissolution. The sealed vial was immersed in a water bath at 37 °C for 1 min before opening (allowing for water condensation) and certain amount of protein was pipetted in to achieve final protein concentration of 30 µM. For protein-gel association studies, stock solutions of proteins were prepared in PBS (Bovine Serum Albumin 27 mg/ml, Lysozyme 5.75 mg/ml, β-lactoglobulin, Insulin 2 mg/ml) and 40 µl of protein stock solution was pipetted into 500 µl of gelator at 37 °C. For the Real Time Fluorescence Microscopy and the *in vivo* study 13.5 mg/ml stock solution of Cy5-BSA in PBS (the labelling protocol is described further below) were prepared and 48 µl of protein stock solution were pipetted into 552 µl gelator (37 °C), then a stock solution of 5 mg/ml DiI in ethanol was prepared and 3 µl were pipetted into 600 µl of warm gelator.

4.3. Release studies of proteins

500 µL of gel containing protein in 2 ml HPLC vials were incubated with 1 ml PBS at 37 °C. The supernatant was removed at different time points (1, 2, 4, 6, 14 and 24 h) and replaced with fresh PBS. The protein concentration was determined using the Bradford colorimetric assay [41]. For lysozyme and β-lactoglobulin, 20 µl of supernatant at each time point was premixed with 200 µl Bradford reagent, for Bovine Serum Albumin 20 µl of supernatant were premixed with 200 µl of Bradford reagent and for Insulin 100 µl of supernatant with 100 µl of Bradford reagent and absorbance at 595 nm was measured using a Tecan Spark 10 M/ 20 M plate reader. Ratios of supernatant: reagent were determined in order to provide with a linear calibration curve (Supplementary Information Fig. S11). For each data point an average of 4 repeats is presented for the calibration curve and an average of 3 repeats for the protein release study.

4.4. Gel degradation study

500 µL of gel in 2 ml HPLC vials were incubated with 1 ml PBS at 37 °C. The supernatant was removed at different time points (the same as the protein release study; 1, 2, 4, 6, 14 and 24 h) and replaced with fresh PBS. 40 µl of supernatant were premixed with 160 µl of methanol and the absorbance was measured at 295 nm in a quartz 96 well-plate using a Tecan Spark 10 M/ 20 M plate reader. For each data point an average of 4 repeats is presented for the calibration curve (Supplementary Information Fig. S9) and an average of 3 repeats for the gel degradation study.

4.5. Fluorescence spectroscopy

600 µL of gel (with or without proteins prepared as explained above) were added to a 2 mm path length cuvette. Fluorescence spectra were recorded at a Cary Eclipse fluorescence spectrophotometer. The spectra were recorded with a scan rate of 30 nm/min, averaging time 1 s, and data interval 0.5 nm using different emission and excitation slits; for BSA (excitation slit 2.5 nm and emission slit 5 nm), β-lactoglobulin (excitation slit 5 nm and emission slit 5 nm), lysozyme (excitation slit 2.5 nm and emission slit 5 nm), insulin (excitation slit 5 nm and emission slit 5 nm). Samples were excited in all cases at 275 nm and 295 nm. Gels (concentration 5 mg/ml) with proteins (30 µM) were prepared and compared to protein solution in PBS (30 µM for all proteins apart from insulin that is 3 µM).

4.6. Fluorescence microscopy

15 µl of warm gelator solution (concentration 0.5% w/v) where the encapsulating molecule has already been added were pipetted in the well and the first image (t = 0 min) was recorded. 400 µl of PBS were added and the well was transferred to 37 °C and images were recorder at t = 10 min, 24 h, 48 h.

Gels were made and imaged in Cellview multiwell, glass bottom

slides (0.17 mm, category 1.5, product no: 543079). Fibers / gels and suspensions were visualized and scanned with the confocal unit of a Zeiss Elyra PS1 LSM780 microscope. Two different objectives were used, water immersion C-Apochromat 63x/1.2 W Korr M27 for scanning the gels and solutions labelled with fluorescamine, and alpha-Plan-Apochromat 100x/1.46 oil objective for Dil and Cy5 labelled proteins and time laps experiments. Fluorescent dyes were detected with the following settings: for fluorescamine, 405 nm laser was set to 0.8%, emission detected at: 490–624 nm, channel colour (LUT) was set to green; for Cy5 labelled proteins, 647 nm laser was set to 4%, emission detected at 654–752 nm, channel colour (LUT) was set to magenta; for Dil, 561 nm laser was set to 0.1%, emission detected at 561–624 nm. To reduce noise, and reveal more details, for all the scans line averaging of 2, and slow scan of 6.3 µs dwell time was applied during scanning. Images and videos were exported using Zeiss Zen 2012 SP5, histogram values (display of the image brightness) was set to the same for the samples belonging to the same experiment.

4.7. Protein labelling

0.4 mg Cyanine5 NHS ester were dissolved in 200 µl DMSO and 6 mg Bovine Serum Albumin were dissolved in 1800 µl NaHCO$_3$ 0.1 M (pH 8.3). The reaction was left under stirring overnight and the mixture was left to dialyse for 7 days using a 3.5 kDa dialysis tubing. After dialysis, the labelled protein was analysed by size exclusion chromatography (SEC) using a TSK gel G3000SWXL (300 × 7.8 mm) column (TOSOH, Tokyo, Japan), running on a HPLC system. The protein was isocratically eluted in DPBS at a flow rate of 1 ml min^{-1}. Fluorescence was recorded at λ_{em} =666 nm, with excitation fixed at λ_{ex} =644 nm. The chromatogram is presented in Fig. S14.

4.8. Enzymatic degradation study

120 µL of warm gelator solution (0.5% w/v) in different buffers [50 mM KH2PO4 (pH = 4.5) for pepsin and PBS for chymotrypsin] were pipetted into 1.5 ml plastic Eppendorf tubes and Bovine Serum Albumin (in PBS) was added, as described earlier, to achieve a final concentrations of 30 µM. 10 µL (5 mg/ml) of pepsin and 20 µl (2 mg/ml) were pipetted on top of the already formed gel and incubated for 1 h, 4 h and 24 h at 37 °C. Enzyme concentrations were selected in order to allow us to qualitatively assess the prevention of protein degradation, in a time course of 24 h. At the previously mentioned time points, the enzymes were quenched after the addition of 80 µl SDS-PAGE Reducing Sample Buffer (RSB), plus 10 µl of HCl 1 M in the case of chymotrypsin, and the samples were denatured by heating at 100 °C for 5 min prior to gel loading. 10 µL of sample were pipetted into a 4–20% Mini-PROTEAN® TGX™ Precast Protein Gel which was run in a standard running buffer (25 mM Tris, 192 mM glycine, 0.1% SDS). Gels were incubated in InstantBlue® (Expedeon, UK). RSB contained 75 mM Tris–HCl pH 6.8, 10% glycerol, 2% SDS, 0.05% bromophenol blue, 2.5% β-mercaptoethanol.

4.9. Samples for dmall angle X-ray scattering (SAXS)

Samples for small angle X-ray scattering (SAXS) were prepared in 1.5 mm borosilicate glass capillaries (Capillary Tube Supplies Ltd) and sealed with a UV-curable adhesive (Norland Optical Adhesive). SAXS measurements were taken on a SAXSLab Ganesha 300XL instrument using a CuKα source (1.54 Å) and a Pilatus 300 K detector. Data collection was performed over a Q range of 0.007–0.25 Å^{-1}, with an exposure time of 7200 s per sample. A correction for tube thickness and curvature was applied during measurement, and a capillary of buffer was run in order to perform background subtraction. The data were fitted using the SasView 4.1 software package.

4.10. Atomic force microscopy

Gel solutions were prepared as previously described for the gel degradation study (see 'Gel degradation study' section). The supernatant after 4 h incubation was extracted and 40 µl were pippeted onto mica. Mica was transferred on preheated at 37 °C AFM stage. Adequate amount (approximately 50 µl) of PBS were added to immerse fully the AFM tip in liquid. Imaging was performed under Peak Force mode using the Bruker FastScan Dimension with ScanAnalyst AFM.

4.11. Lysozyme functionality assay

A turbidimetric enzymatic assay was performed by measuring the decrease in optical density of an aqueous suspension of Micrococcus lysodeikticus lyophilised cells, a natural substrate for lysozyme, in PBS. Gel with lysozyme was prepared as described before and 0.5 ml of gel was incubated with 1 ml of PBS at 37 °C for 24 h until gel erosion. The final concentration of lysozyme in the dispersion produced was 37 µg/mL. PBS (20 mL) solution was added to 10 mg of lyophilised cells. 300 µl of this substrate suspension were added to 150 µl of solution and the decrease in optical density at λ =460 nm was measured as a function of time. Free gelator and free lysozyme were used as controls at the same concentration as in the samples after incubation at the same conditions as lysozyme in the gel. All kinetic experiments were carried out in triplicate.

4.12. Evaluation of the insulin bioactivity in human cells

The HepG2 cell line was obtained from ECACC (UK, distributed by SIGMA) and cultured in growth medium: EMEM (1 g glucose/L, SIGMA, UK) supplemented with 10% FBS (GIBCO, Thermo South America), 1% Non-essential amino acids (GIBCO, Thermo Grand Island USA), 2 mM L-Glutamine (SIGMA Brazil), 1% Penicillin-Streptomycin (SIGMA Israel). HepG2 originated from a human liver carcinoma, a bona-fide insulin target organ, and are enriched in Insulin Receptor expression (https://www.proteinatlas.org/ENSG00000171105-INSR/cell). Cells were passaged once per week by trypsinization (10x Trypsin solution, SIGMA USA) for 5 min and passage through an 18 gauge needle to obtain a single cell suspension. They were used between passages 3 and 20.

For transfection, Viafect (Promega, Madison USA), and Turbofect (Thermo, Lithuania) were compared by measuring the efficiency of transfection of a commercial plasmid preparation of pMAXGFP (Lonza, Köhln Germany) following the standard recommended protocols. Efficiency was calculated measuring the number of GFP fluorescent cells respect to the total number of cells stained with Hoescht 33258 (SIGMA Israel). Apoptosis measured as condensed Hoescht + cells was also measured and discarded for efficiency. Since Viafect obtained a > 95% efficiency while Turbofect approached 65%, all subsequent experiments were performed using Viafect.

MW48 plates (Costar, Thermo NY USA) were previously coated with 100 µg/ml Type I collagen solution in PBS (stock solution: 4 mg/ml, SIGMA St Louis MO USA) and washed three times with PBS (SIGMA St Louis MO USA). For each assay, 24000 HepG2 cells/well were seeded on these wells in growth medium, and allowed to grow for one full day. Next day, a transfection mix of DNA plasmid (85 ng of promoter + 35 ng empty RSV plasmid/well), Viafect transfection reagent (1.5 µL/well) and EMEM (23.5 µL/well) was prepared for all wells combined and incubated for 20 min. The plasmids used were: pSynSRE-T-luc (Addgene, Cambridge USA) containing the − 324 to − 225 bp fragment of the hamster HMG-CoA synthase promoter containing the SRE elements upstream of the minimal HMG-CoA synthase TATA box (− 28 to + 39) pSynSRE-Mut-T-luc bearing four point mutations in that promoter SRE elements [44,45]. It has been previously shown that Insulin regulates HMG-CoA synthase expression through those SRE sites in human cells, and its action abolished in the mutated promoter [46].

Meanwhile, cell medium was replaced by growth medium plus

2 mM metformin (SIGMA, Steinheim Germany). Metformin helps to reduce the basal luciferase expression while the cells were under transfection. Subsequently, 25 μl of the transfection mix was pipetted per well and incubated during 6 h. After three washes with warm PBS were performed and changed to deprived medium (as growth medium but with only 0.5% FBS) including the insulin/vehicle to test (5–200 μIU/ml or equivalent vehicle volume). Each condition was tested in six-eight replicates. After 20 h, wells were washed three times with PBS followed by addition of 40 μl PassiveLysis Buffer/well (Promega, Madison USA) for 20 min. Lysates were collected and frozen at − 20 °C. Luciferase activity was assayed as described[56] using 15 μL of lysate in a Mithras microplate reader (LB940, Berthold, Bad Wildbad Germany). Experiments were repeated three times.

Statistics and figures were performed with GraphPad 7 by applying first a Kolmogorov-Smirnov normality test and, being normally distributed, following by an unpaired *t-test* to assess significance. Insulin –Vehicle concentrations were plotted in parallel graphics comparing the normal SynSRE-T-luc and the mutated SynSRE-Mut-T-luc promoter (SI, Fig. S6).

4.13. Rheology studies

Rheology was carried out using an Anton Paar MCR302 Modular Compact Rheometer. A four bladed vane geometry was used with a diameter of 8.5 mm and length 8.5 mm in a cup with a diameter of 14.5 mm. The solution of gelator was prepared in 7 ml aluminium cups to a final sample volume of 2 mL, as per the method described above. Once the gel was prepared, the sample vial was mounted in the lower plate (cup) of the rheometer; the vane (attached to the upper part) was lowered into place, at a depth of 2 mm. This arrangement gave a total sample depth of approximately 16 mm in the 14.5 mm diameter cup which allowed positioning of the vane in the centre of the sample. All rheological measurements were carried out in 7 ml aluminium vials to allow for heating at 37 °C of the sample prior to measurement. Time dependant recovery measurements were carried out by alternating the strain between 5% and 500%; conditions that could guarantee a stable gel at the lower strain and complete deformation at the higher strain. The strains were applied in 20 min (0.2%) and 30 s (500%), followed by 30 min (0.2%) cycles. The frequency (5 rad/sec) and temperature (37 °C) were kept constant throughout.

4.14. In vivo study

This study was conducted under the Animals (Scientific Procedures) Act 1986 UK Home Office Licence number PPL P435A9CF8, 19b and given ethical approval by the University of Nottingham AWERB. NCRI guidelines for the welfare and use of animals in cancer research, LASA good practice guidelines and FELASA working group on pain and distress guidelines were followed. ARRIVE Guidelines were followed in the reporting of the animal studies. 12 female CD-1 NuNu mice (12 weeks old) were obtained from Charles River (UK). Mice were maintained in IVCs (Tecniplast UK) within a barriered unit illuminated by fluorescent lights set to give a 12 h light-dark cycle (on 07.00, off 19.00), as recommended in the United Kingdom Home Office Animals (Scientific Procedures) Act 1986. The room was air-conditioned by a system designed to maintain an air temperature range of 21 ± 2 °C and a humidity of 55% + 10%. Mice were housed in social groups during the procedure with irradiated bedding and provided with autoclaved nesting materials and environmental enrichment. Daily monitoring of general health and well-being and weights was undertaken.

After injections of the different formulations, fluorescence signal was measured at 0 h, 1 h, 2 h, 4 h, 24 h and 72 h followed by weekly imaging through IVIS Spectrum. The gels were prepared with a concentration 5 mg/ml of gelator, 0.025 mg/ml Dil or 1 mg/ml Cy5-BSA. The gel containing Dil contained 0.5% v/v ethanol in order to solubilise the hydrophobic dye. 4 different groups of mice were used: (1) gels containing Dil, (2) gels containing Cy5-BSA, (3) gel alone, and (4) Cy5-BSA in solution.

For the data processing the Living Image Software was used. Rectangular regions of interest (ROI) were drawn including the area occupied by the gel at t = 0 h. The same ROIs were used for the other time points. Fluorescence intensity values were extracted in radiance ($\rho/sec/cm^2/sr$) and presented in the same colour scale.

4.15. Inflammation markers at the site of injection

Skin was excised from around the injection site including the area in which the gel had resided. All samples (samples with gel, N = 3 and a control with no gel injected) were embedded in optimal cutting temperature (OCT) compound using liquid nitrogen cooled isopentane. Serial sections 7 μm thick were cut from each block throughout the entire tissue on a crystat (Leica, Germany) and mounted on polysilinated microscope glass slides (Menzel Gläser Polysine®; Thermo-Scientific, Germany). Following embedding and sectioning, tissue sections were fixed in 4% paraformaldehyde for 5 min and stained using haematoxylin and eosin (H&E). H&E staining was achieved by immersing samples for 2.5 min in haematoxylin, 15 s in 1% acetic industrial methylated spirits, 15 s in ammoniated water and 4 min in eosin. Following staining were dehydrated through an ethanol series (50, 70, 90, 95 and 100% ethanol for 5 min each followed by 2X xylene immersions) and glass coverslips were mounted using DPX. Following staining, tissue and cell morphology was analysed throughout the tissue samples. The observer was blinded to the sample identification to avoid subconscious bias. Images were captured using a Leica CTR500 microscope (Leica Microsystems, Germany) with bright field light. For each sample several sections 200 μm apart were analysed at 5X, 10X, 20X, 40X and 60X magnifications and photomicrographs captured.

Acknowledgements

Appendix A. Supplementary data

Supplementary material related to this article can be found, in the online version, at doi:https://doi.org/10.1016/j.jconrel.2019.10.011. Raw data created during this research are openly available from the corresponding authors (maria.marlow@nottingham.ac.uk, mischa.zelzer@nottingham.ac.uk) and at the University of Nottingham Research Data Management Repository (https://rdmc.nottingham.ac.uk/) https://doi.org/10.17639/nott.7026.

References

[1] A.S. Hoffman, Hydrogels for biomedical applications, Adv. Drug Deliv. Rev. 64 (2012) 18–23.
[2] P. Gupta, K. Vermani, S. Garg, Hydrogels: from controlled release to pH-responsive drug delivery, Drug Discov. Today 7 (10) (2002) 569–579.
[3] Y. Qiu, K. Park, Environment-sensitive hydrogels for drug delivery, Adv. Drug Deliv. Rev. 53 (3) (2001) 321–339.
[4] P. Flory, Introductory lecture, Faraday Discuss. Chem. Soc. 57 (1974) 7–18.

[5] Y. Li, F. Wang, H. Cui, Peptide-based supramolecular hydrogels for delivery of biologics, Bioeng. Transl. Med. 1 (3) (2016) 306–322.

[6] T. Christoff-Tempesta, A.J. Lew, J.H. Ortony, Beyond covalent crosslinks: applications of supramolecular Gels, Gels 4 (2) (2018) 40.

[7] K.J. Skilling, et al., Insights into low molecular mass organic gelators: a focus on drug delivery and tissue engineering applications, Soft Matter 10 (2) (2014) 237–256.

[8] H. Cui, M.J. Webber, S.I. Stupp, Self-assembly of peptide amphiphiles: from molecules to nanostructures to biomaterials, Pept. Sci. 94 (1) (2010) 1–18.

[9] T. Vermonden, R. Censi, W.E. Hennink, Hydrogels for protein delivery, Chem. Rev. 112 (5) (2012) 2853–2888.

[10] R.J. Mart, et al., Peptide-based stimuli-responsive biomaterials, Soft Matter 2 (10) (2006) 822–835.

[11] G.M. Peters, J.T. Davis, Supramolecular gels made from nucleobase, nucleoside and nucleotide analogs, Chem. Soc. Rev. 45 (11) (2016) 3188–3206.

[12] T. Tokunou, et al., Engineering insulin-like growth factor-1 for local delivery, Faseb J. 22 (6) (2008) 1886–1893.

[13] H. Guo, et al., Sustained delivery of VEGF from designer self-assembling peptides improves cardiac function after myocardial infarction, Biochem. Biophys. Res. Commun. 424 (1) (2012) 105–111.

[14] A. Nishimura, et al., Controlled release of insulin from self-assembling nanofiber hydrogel, PuraMatrix™: application for the subcutaneous injection in rats, Eur. J. Pharm. Sci. 45 (1–2) (2012) 1–7.

[15] G. Liang, et al., Supramolecular hydrogel of a D-amino acid dipeptide for controlled drug release in vivo, Langmuir 25 (15) (2009) 8419–8422.

[16] X. Li, et al., Introducing D-amino acid or simple glycoside into small peptides to enable supramolecular hydrogelators to resist proteolysis, Langmuir 28 (37) (2012) 13512–13517.

[17] X. Li, et al., Supramolecular hydrogels formed by the conjugates of nucleobases, Arg-Gly-Asp (RGD) peptides, and glucosamine, Soft Matter 8 (28) (2012) 7402–7407.

[18] M.A. Ramin, et al., Low molecular weight hydrogels derived from urea based-bolaamphiphiles as new injectable biomaterials, Biomaterials 145 (2017) 72–80.

[19] J. Kaplan, P. Barthélémy, M. Grinstaff, Self-assembled nanofiber hydrogels for mechanoresponsive therapeutic anti-TNFα antibody delivery, Chem. Commun. 52 (34) (2016) 5860–5863.

[20] M.A. Ramin, et al., Cation tuning of supramolecular gel properties: a new paradigm for sustained drug delivery, Adv. Mater. 29 (13) (2017) 1605227.

[21] N. Sreenivasachary, J.M. Lehn, Structural selection in G-Quartet-based hydrogels and controlled release of bioactive molecules, Chem.–An Asian J. 3 (1) (2008) 134–139.

[22] T.N. Plank, J.T. Davis, AG 4· K+ hydrogel that self-destructs, Chem. Commun. 52 (28) (2016) 5037–5040.

[23] M.C. Branco, et al., Macromolecular diffusion and release from self-assembled β-hairpin peptide hydrogels, Biomaterials 30 (7) (2009) 1339–1347.

[24] M.C. Branco, et al., The effect of protein structure on their controlled release from an injectable peptide hydrogel, Biomaterials 31 (36) (2010) 9527–9534.

[25] S. Koutsopoulos, et al., Controlled release of functional proteins through designer self-assembling peptide nanofiber hydrogel scaffold, Proc. Natl. Acad. Sci. U.S.A. 106 (12) (2009) 4623–4628.

[26] L. Johnson, et al., Low molecular weight nucleoside Gelators: a platform for protein aggregation inhibition, Mol. Pharm. 16 (1) (2019) 462–467.

[27] M. Conejero-Muriel, et al., Influence of the chirality of short peptide supramolecular hydrogels in protein crystallogenesis, Chem. Commun. 51 (18) (2015) 3862–3865.

[28] S. Kiyonaka, et al., Semi-wet peptide/protein array using supramolecular hydrogel, Nat. Mater. 3 (2003) 58.

[29] G. Scott, et al., Pickering stabilized peptide gel particles as tunable microenvironments for biocatalysis, Langmuir 29 (46) (2013) 14321–14327.

[30] J.M. Barichello, et al., Absorption of insulin from Pluronic F-127 gels following subcutaneous administration in rats, Int. J. Pharm. 184 (2) (1999) 189–198.

[31] P.L. Wang, T.P. Johnston, Sustained-release interleukin-2 following intramuscular injection in rats, Int. J. Pharm. 113 (1) (1995) 73–81.

[32] K.J. Skilling, et al., Developing a self-healing supramolecular nucleoside hydrogel, Soft Matter 12 (43) (2016) 8950–8957.

[33] M. Angelerou, et al., A supramolecular nucleoside-based gel: molecular dynamics simulation and characterization of its nanoarchitecture and self-assembly mechanism, Langmuir (2018) 6912–6920.

[34] S. Udenfriend, et al., Fluorescamine: a reagent for assay of amino acids, peptides, proteins, and primary amines in the picomole range, Science 178 (4063) (1972) 871–872.

[35] C.A. Royer, Probing protein folding and conformational transitions with fluorescence, Chem. Rev. 106 (5) (2006) 1769–1784.

[36] J.-B. Guilbaud, A. Saiani, Using small angle scattering (SAS) to structurally characterise peptide and protein self-assembled materials, Chem. Soc. Rev. 40 (3) (2011) 1200–1210.

[37] M.G.F. Angelerou, et al., Hydrophobicity of surface-immobilised molecules influences architectures formed via interfacial self-assembly of nucleoside-based gelators, Soft Matter 14 (48) (2018) 9851–9855.

[38] S. Soukasene, et al., Antitumor activity of peptide Amphiphile nanofiber-encapsulated camptothecin, ACS Nano 5 (11) (2011) 9113–9121.

[39] L. Gráf, L. Szilágyi, I. Venekei, Chymotrypsin, Handbook of Proteolytic Enzymes, 3rd ed., Elsevier, 2013, pp. 2626–2633.

[40] M.E. Smith, D.G. Morton, The Digestive System: Systems of The Body Series, Elsevier Health Sciences, 2011.

[41] N.J. Kruger, The Bradford method for protein quantitation, The Protein Protocols Handbook, Springer, 2002, pp. 15–21.

[42] J. Berg, et al., Biochemistry, ed 5th, WH Freeman, New York, 2002.

[43] D. Shugar, The measurement of lysozyme activity and the ultra-violet inactivation of lysozyme, Biochim. Biophys. Acta 8 (C) (1952) 302–309.

[44] K.A. Dooley, S. Millinder, T.F. Osborne, Sterol regulation of 3-hydroxy-3-methyl-glutaryl-coenzyme A synthase gene through a direct interaction between sterol regulatory element binding protein and the trimeric CCAAT-binding factor/nuclear factor Y, J. Biol. Chem. 273 (3) (1998) 1349–1356.

[45] J.R. Smith, et al., Multiple sterol regulatory elements in promoter for hamster 3-hydroxy-3-methylglutaryl-coenzyme A synthase, J. Biol. Chem. 263 (34) (1988) 18480–18487.

[46] I.R. Harris, et al., Regulation of HMG-CoA synthase and HMG-CoA reductase by insulin and epidermal growth factor in HaCaT keratinocytes, J. Invest. Dermatol. 114 (1) (2000) 83–87.

[47] Mayo Clinic Laboratory, Serum Insulin Range of Values for Normal Population at Fasting, Available from: https://www.mayomedicallaboratories.com/test-catalog/Clinical + and + Interpretive/62990.

[48] S. Melmed, et al., Williams Textbook of Endocrinology, Saunders Elsevier, Philadelphia, PA, 2011.

[49] A.R. Rees, M.J. Sternberg, From Cells to Atoms: an Illustrated Introduction to Molecular Biology, (1984).

[50] S.B. Bravo, et al., Humanized medium (h7H) allows long-term primary follicular thyroid cultures from human normal thyroid, benign neoplasm, and cancer, J. Clin. Endocrinol. Metab. 98 (6) (2013) 2431–2441.

[51] A.R. Son, et al., Direct chemotherapeutic dual drug delivery through intra-articular injection for synergistic enhancement of rheumatoid arthritis treatment, Sci. Rep. 5 (2015) 14713.

[52] J.M. Anderson, M.S. Shive, Biodegradation and biocompatibility of PLA and PLGA microspheres, Adv. Drug Deliv. Rev. 28 (1) (1997) 5–24.

[53] J.M. Anderson, In vivo biocompatibility of implantable delivery systems and biomaterials, Eur. J. Pharm. Biopharm. 40 (1) (1994) 1–8.

[54] A. Motulsky, et al., Characterization and biocompatibility of organogels based on L-alanine for parenteral drug delivery implants, Biomaterials 26 (31) (2005) 6242–6253.

[55] J.M. Anderson, Biological responses to materials, Annu. Rev. Mater. Res. 31 (1) (2001) 81–110.

[56] A. Garcia-Rendueles, et al., Rewiring of the apoptotic TGF-β-SMAD/NFκB pathway through an oncogenic function of p27 in human papillary thyroid cancer, Oncogene 36 (5) (2017) 652.